JACS
JOURNAL OF THE AMERICAN CHEMICAL SOCIETY

Subscriber access provided by American Chemical Society

Article

Molecular Dynamics Simulation of the Formation, Structure, and Dynamics of Small Phospholipid Vesicles

Siewert J. Marrink, and Alan E. Mark

J. Am. Chem. Soc., **2003**, 125 (49), 15233-15242• DOI: 10.1021/ja0352092 • Publication Date (Web): 13 November 2003

Downloaded from http://pubs.acs.org on March 30, 2009

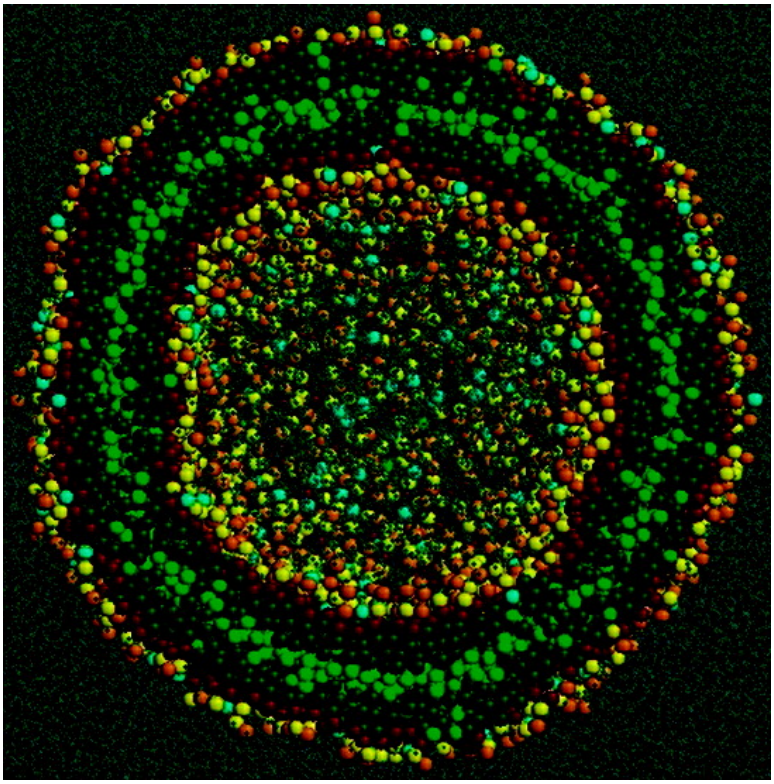

More About This Article

Additional resources and features associated with this article are available within the HTML version:

- Supporting Information
- Access to high resolution figures
- Links to articles and content related to this article
- Copyright permission to reproduce figures and/or text from this article

ACS Publications
High quality. High impact.

Journal of the American Chemical Society is published by the American Chemical Society. 1155 Sixteenth Street N.W., Washington, DC 20036

JACS
JOURNAL OF THE AMERICAN CHEMICAL SOCIETY

Subscriber access provided by American Chemical Society

View the Full Text HTML

ACS Publications
High quality. High impact.

Journal of the American Chemical Society is published by the American Chemical Society. 1155 Sixteenth Street N.W., Washington, DC 20036

J|A|C|S
ARTICLES
Published on Web 11/13/2003

Molecular Dynamics Simulation of the Formation, Structure, and Dynamics of Small Phospholipid Vesicles

Siewert J. Marrink* and Alan E. Mark

Contribution from the Department of Biophysical Chemistry, University of Groningen, Nijenborgh 4, 9747 AG Groningen

Received March 18, 2003; E-mail: marrink@chem.rug.nl

Abstract: Here, we use coarse grained molecular dynamics (MD) simulations to study the spontaneous aggregation of dipalmitoylphosphatidylcholine (DPPC) lipids into small unilamellar vesicles. We show that the aggregation process occurs on a nanosecond time scale, with bicelles and cuplike vesicles formed at intermediate stages. Formation of hemifused vesicles is also observed at higher lipid concentration. With either 25% dipalmitoylphosphatidylethanolamine (DPPE) or lysoPC mixed into the system, the final stages of the aggregation process occur significantly faster. The structure of the spontaneously formed vesicles is analyzed in detail. Microsecond simulations of isolated vesicles reveal significant differences in the packing of the lipids between the inner and outer monolayers, and between PC, PE, and lysoPC. Due to the small size of the vesicles they remain almost perfectly spherical, undergoing very limited shape fluctuations or bilayer undulations. The lipid lateral diffusion rate is found to be faster in the outer than in the inner monolayer. The water permeability coefficient of the pure DPPC vesicles is of the order of 10^{-3} cm s^{-1}, in agreement with experimental measurements.

1. Introduction

Solutions of lipid molecules exhibit a large variety of aggregation states. One of these possible aggregation states is vesicular, in which the lipids form a spherically closed bilayer, i.e., a vesicle or a liposome. Such vesicles are important model systems for biological cells. They are also used for drug delivery among other applications.

The formation of vesicles using computer simulation techniques was first studied by Drouffe et al.[1] Their lipids were modeled as single particles, with anisotropic pair interactions and a multibody hydrophobic driving force. Molecular dynamics simulations show spontaneous aggregation of such particles into vesicles. A more realistic lipid model consisting of three connected particles (one modeling the headgroup, two modeling the tail) was recently used to study vesicle formation by Noguchi and Takasu[2] using Brownian dynamics. Explicit solvent was included for the first time in a dissipative particle dynamics (DPD) study of vesicle formation by Yamamoto.[3] In DPD, the lipids are modeled as soft beads connected by springs. Several lipid geometries were simulated using both random and bilayer like starting conditions. Vesicle formation was observed in each case. Although the models and simulation techniques used by the different groups cited above differ considerably, vesicle formation is observed in each case to proceed via a bicellar like intermediate. Once formed, the bicelle encapsulates water and eventually forms a closed vesicle.

The mechanism of vesicle formation from random solutions appears to not be very model dependent, and simple stochastic models seem adequate to obtain a qualitative understanding. However, for a more quantitative understanding of the process, a more detailed model is warranted. Fully atomistic simulations can accurately reproduce experimental quantities for explicit lipids, but are currently limited to small scale aggregation processes such as bilayer formation.[4] To bridge the gap between specific atomistic simulations and aspecific stochastic modeling, we developed a new coarse grained (CG) model suitable for MD simulations. The model is based on atomistic simulations and therefore accurate in its predictions of properties of bilayer aggregates. Nevertheless, the model is fast enough to allow large scale lipid simulations including explicit solvent.

In this paper, we use this model to study the aggregation of dipalmitoylphosphatidylcholine (DPPC) into vesicles. DPPC is a typical phospholipid of biological membranes, and well studied both experimentally and computationally. Experimentally, small unilamellar vesicles of DPPC are usually obtained by sonication. The minimal size of such vesicles is about 20 nm in diameter.[5] This is comparable to the size of the vesicles formed in our simulations. We also study the formation of vesicles in mixed DPPC/DPPE (dipalmitoylphosphatidylethanolamine) and DPPC/lysoPC systems. Experiments show that lipids with headgroups that favor phases with negative curvature, such as PE, can stabilize intermediates with inverted type structure and, likewise, destabilize intermediates with positive curvature (for a review, see ref 6). The opposite effect is seen for lysolipids, which induce positive curvature into the system.

(1) Drouffe, J. M.; Maggs, A. C.; Leibler, S. *Science* **1991**, *254*, 1353.
(2) Noguchi, H.; Takasu, M.; *Phys. Rev.* **2001**, *E 64*, 1.
(3) Yamamoto, S.; Maruyama, Y.; Hyodo, S.; *J. Chem. Phys.* **2002**, *116*, 5842.
(4) Marrink, S. J.; Lindahl, E.; Edholm, O.; Mark, A. E.; *J. Am. Chem. Soc.* **2001**, *123*, 8638.
(5) Cornell, B. A.; Fletcher, G. C.; Middlehurst, J.; Separovic, F. *Biochim. Biophys. Acta* **1982**, *690*, 15.

10.1021/ja0352092 CCC: $25.00 © 2003 American Chemical Society

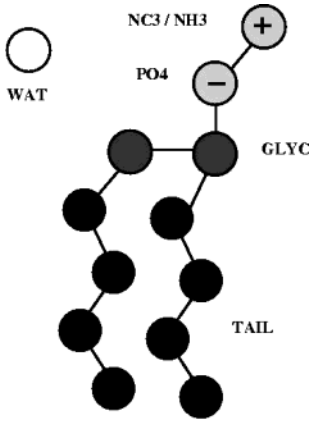

Figure 1. Structure and nomenclature of the molecules in the coarse grained model.

Table 1. Interaction Matrix: Level of Interaction I (attractive, $\epsilon = 5$ kJ/mol), II (semi-attractive, $\epsilon = 4.2$ kJ/mol), III (intermediate, $\epsilon = 3.4$ kJ/mol), IV (semi-repulsive, $\epsilon = 2.6$ kJ/mol) or V (repulsive, $\epsilon = 1.8$ kJ/mol)

group	WAT	NC3/PO4	NH3	GLYC	TAIL
WAT	I	I	I	III	V
NC3/PO4	I	III	I	III	V
NH3	I	I	II	II	V
GLYC	III	III	II	II	IV
TAIL	V	V	V	IV	III

The remainder of the paper is organized as follows. The section on methodology describes in detail the CG force field used in the simulations and the systems simulated. The results are presented in four parts: the first part describes the spontaneous aggregation process of lipids to form vesicles, the second part provides details about the structure of pure DPPC vesicles, the third part shows the changes in structure for vesicles containing PE or lysoPC, and the fourth part provides some results on vesicle dynamics. This is followed by a general discussion in which we present a simplistic model of lipid packing inside vesicles. Finally the main conclusions are briefly summarized.

2. Methods

2.1 Model. In our coarse-grained model, DPPC and DPPE are represented by twelve coarse grained atoms, as shown in Figure 1. The headgroup consists of two hydrophilic groups ("NC3" for the choline group of PC or "NH3" for the amine group of PE, and "PO4" for the phosphate moiety) and two intermediately hydrophilic ones for the glycerol moiety ("GLYC"). Each of the two tails is modeled by four hydrophobic particles (type "TAIL"). LysoPC is modeled as DPPC but with one rather than two tails. The solvent is modeled by individual hydrophilic particles ("WAT") each representing four real water molecules. The coarse grained atoms interact in a pairwise manner via a Lennard−Jones (LJ) potential. Five different LJ potentials are used, ranging from weak (labeled "repulsive", mimicking hydrophobic interactions) to strong (labeled "attractive", for hydrophilic interactions) with three levels in between. The five different interaction strengths are obtained by changing the well depth ϵ only. All CG particles have exactly the same size of $\sigma = 0.47$ nm, and the same mass of 72 amu (corresponding to four water molecules). The LJ parameters used in the simulations are summarized in Table 1.

In addition to the LJ interactions, a screened Coulomb interaction (with $\epsilon_r = 20$) is used to model the electrostatic interaction between the zwitterionic headgroups. The NC3 and the NH3 group both bear a charge of +1, and the phosphate group bears a charge of −1. Both the LJ and Coulomb interactions are only short ranged, however, using a shift based cutoff of 1.2 nm. Soft springs between bonded pairs keep the molecule together. The spring constant $K_{bond} = 1250$ kJ mol^{-1} nm^{-2} with an equilibrium distance of σ. Angle potentials provide the appropriate stiffness for the lipid molecule. A cosine based angle potential is used with a weak force constant $K_{angle} = 25$kJ mol^{-1} rad^{-2} and an equilibrium angle of 180°. This angle potential is used for the triplets GLYC−C1−C2, C1−C2−C3, and C2−C3−C4 for both tails and for PO4−GLYC−C1. An additional angle potential with an equilibrium angle of 120° is furthermore used for the glycerol backbone PO4−GLYC−GLYC.

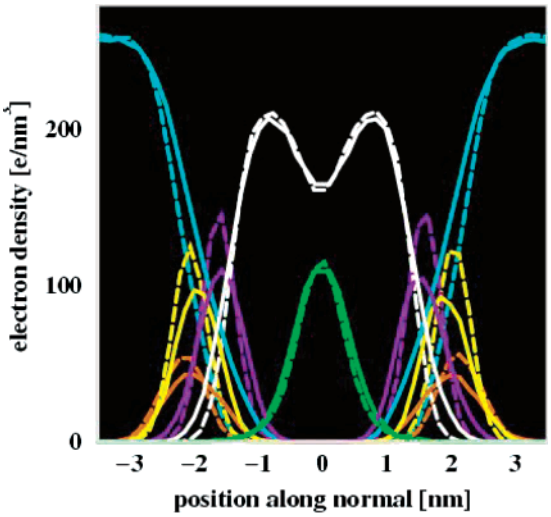

Figure 2. Comparison of electron density distributions obtained from atomistic (solid lines) and coarse grained (dashed) simulations. The water density is shown in blue, the density of NC3 groups in orange, PO4 groups in yellow, the glycerol backbone in purple, and the terminal tail groups in green. The total tail density is shown in white.

The setup of our CG force field is comparable to the recently developed CG lipid force fields of Goetz[7] and Shelley,[8] which are based on the pioneering work of Smit.[9] Extensive optimization of the parameters has resulted in the current CG model, which can be interpreted on a quantitative level. Densities of pure liquids such as water and bulk alkanes are reproduced to within a few percent at room temperature, and mutual solubilities of oil and water mixtures agree to within kT with the available literature values. The current version of our CG force field also represents the lamellar state of many lipids including DPPC and DPPE very well. The area per lipid for DPPC at 323 K is 0.65 nm^2 (experimental 0.64 nm^2 [10]) and for DPPE 0.62 nm^2 at 342 K (experimental 0.605 nm^2.[11] The electron density distributions along the bilayer normal are very close to those obtained with atomistic simulations. This is illustrated in figure 2 which shows the electron density profiles for a number of components as a function of the distance along the membrane normal, both for an atomistic model and our CG model. The atomistic density distributions were obtained from a simulation of a bilayer patch containing 256 DPPC lipids using a standard atomistic lipid force field.[12] To compare to the CG distributions, the center-of-mass of the atomistic groups corresponding to a CG particle were used to calculate the densities, except in the case of water for which this is of course not possible. The CG distributions

(6) Chernomordik, L. V.; Kozlov, M. M.; Zimmerberg, J. *J. Membr. Biol.* **1995**, *146*, 1.
(7) Goetz, R.; Gompper, G.; Lipowsky, R. *Phys. Rev. Lett.* **1999**, *82*, 221.
(8) Shelley, J. C.; Shelley, M.; Reeder, R.; Bandyopadhyay, S.; Klein, M. L. *J. Phys. Chem. B* **2001**, *105*, 4464.
(9) Smit, B.; Hilbers, P. A. J.; Esselink, K.; Rupert, L. A. M.; Van Os, N. M.; Schlijper, A. G. *J. Phys. Chem.* **1991**, *95*, 6361.
(10) Nagle, J. F.; Tristram-Nagle, S. *Biochim. Biophys. Acta* **2000**, *1469*, 159.
(11) Petrache, H. I.; Dodd, S.; Brown, M. *Biophys. J.* **2000**, *79*, 3172.
(12) Lindahl, E.; Edholm, O. *Biophys. J.* **2000**, *79*, 426.

were obtained also from a 256 DPPC bilayer simulation. Both CG and atomistic simulations were performed at the same temperature as the simulations of vesicle formation ($T = 323$ K) and at conditions of zero surface tension. The peaks of the distributions can be observed to coincide to within 0.1 nm, for each of the membrane components. Only the water penetrates the bilayer to a somewhat larger extent in the atomistic simulations, but this is mainly a result of the representation of four realistic water molecules by the center of a single CG solvent particle. If the density would be smeared out equally across the diameter of the CG particle (almost 0.5 nm), then the depth of water penetration becomes very similar. The interface in the CG model is slightly more structured than in the atomistic model, however. The thickness of the CG bilayer, measured from the peaks of the phosphate distribution, measures 4.0 ± 0.1 nm, close to the experimentally determined bilayer thickness of 3.85 nm for the lamellar phase of DPPC in the liquid-crystalline phase.[10] Apart from the ability to reproduce important structural quantities, collective properties such as the bending modulus, area compressibility, and line tension are important parameters to judge the quality of the model. Analysis of the undulatory modes of a large coarse grained DPPC bilayer slab (6400 lipids) reveals a bending modulus of $4 \pm 2 \times 10^{-20} J$, which is close to the value of $5.6 \pm 0.6 \times 10^{-20} J$ obtained experimentally for DMPC.[13] From the fluctuations in the membrane area, the area compressibility is found to be 260 ± 40 mN/m. This value compares well with the experimental value for DPPC which is reported to be 231 ± 20 mN/m.[10] Also the line tension of $5 \pm 1 \times 10^{-11} N$, estimated from the critical tension at which pores can be stabilized in a DPPC bilayer, is of the same order of magnitude as the estimates from experiments $1 \times 10^{-11} N$[14] and from atomistic simulations ($1-3 \times 10^{-11} N$).[15]

Because the potential functions of the CG model are smoother compared to atomistic models, the dynamics of CG systems is significantly faster. This is advantageous as it allows faster sampling of the configurational space, but makes the interpretation of the time scale somewhat arbitrary. On the basis of a comparison of diffusion rates of real water and the CG water, the CG model is found to diffuse four times faster. Similar factors are found not only for bulk alkane systems, but also for lipid systems. The relative dynamics in the CG model therefore seems well preserved. To give a physically meaningful time scale, the time scale used to present the results is an effective time, i.e., the actual simulation time multiplied by a factor of 4. With this effective time scale, both the diffusion rate of water molecules ($2 \times 10^{-5} \mathrm{cm^2 s^{-1}}$ at 300 K) and the lateral diffusion rates of lipids ($3 \times 10^{-7} \mathrm{cm^2 s^{-1}}$ for DPPC at 323 K) are close to the experimental estimates (for DPPC, values are typically reported around $1 \times 10^{-7} \mathrm{cm^2 s^{-1}}$ at temperatures close to 323 K, e.g., refs 16, 17). Also the time scales of self-aggregation of lipids into bilayers are comparable to atomistic simulations. Details concerning the development of the CG force field including a more extensive comparison between CG bilayers and atomistic bilayers will be published elsewhere. The parameters and topologies can also be obtained from our web-site at http://md.chem.rug.nl/marrink/coarsegrain.html.

2.2 Simulations. Table 2 gives an overview of the 10 simulations described in this paper. Four of them (RANDOM I−IV) start from a random solution of DPPC molecules in water. The starting conformations for these simulations were generated by solvating 1500 (or 2500) lipids placed randomly in a cubic simulation box of 25 nm edge length. To avoid interference with the boundaries (for which periodic boundary conditions were used) an additional layer of 5 nm width of pure water was added. The total amount of CG water particles is close to 400 000, corresponding to more than 1.5 million water molecules. The total concentration of lipids in the systems RANDOM I−III is ~60 mM (~125 mM in RANDOM IV), but the local concentration in the center of the simulation is about twice as high. The starting structure for the BICEL simulations was obtained from the trajectory of the RANDOM-I simulation, at the stage where a bicelle had just been formed (see Results). This bicelle, consisting of 877 lipids, was isolated including some of the surrounding solvent, and placed into a rhombic dodecahedral box. New random velocity distributions generated quasi-independent starting configurations for three additional simulations of the bicelle to vesicle transition. Randomly replacing 25% of the DPPC molecules by either DPPE or lysoPC molecules (which only requires changing the type of the NC3 group to an NH3 group or deleting one of the two tails) resulted in the starting structure for the mixed systems BICEL-PE-I and BICEL-lysoPC. The starting structure for system BICEL-PE-II was generated differently. An artificial bicelle was cut from a large DPPC bilayer patch and solvated in a rectangular box of $42 \times 42 \times 10$ nm, with the bicellar normal aligned along the smallest axis. Here also, 25% randomly chosen DPPC molecules were replaced by DPPE.

Table 2. Overview of Simulations Performed

label	DPPC (/PE)	water[a]	time[b] (μs)
RANDOM-I	1500	400000	1
RANDOM-II	1500	400000	0.3
RANDOM-III	1500	400000	0.3
RANDOM-IV	2500	300000	0.6
BICEL-I	877	60000	5
BICEL-II	877	60000	0.2
BICEL-III	877	60000	0.2
BICEL-PE-I	658/219	60000	5
BICEL-PE-II	1888/640	125000	0.5
BICEL-lysoPC	658/219	60000	5

[a] number of CG water particles. The corresponding number of real water molecules is four times larger. [b] effective simulation time (see Methods).

All system were subsequently simulated using the GROMACS simulation package[18] with a time step of $t = 200$ fs (effective time scale, 50 fs actual time step). Constant temperature ($T = 323$ K) and pressure ($P = 1$ bar) conditions were applied. At this state point, DPPC remains in the biologically relevant fluid state. Pressure coupling was applied isotropicaly in all cases except for system BICEL-PE-II, for which anisotropic pressure scaling was used to allow the initially rectangular box to deform into a more cubic geometry along with shape transformation of the bicelle into a vesicle. Simulations RANDOM-II and III, and BICEL-II and -III were aborted shortly after the final vesicle had formed. The other simulations were continued up to several microseconds to gather statistics about the vesicle structure, and in order to observe possible long time global structural changes in the solutions.

3. Results

3.1 Spontaneous Aggregation into Vesicles. Figure 3 shows a series of snapshots illustrating the aggregation process during one of the simulations (RANDOM-I). Starting from a random solution (A) of phospholipids, we observe a rapid initial local clustering into micelles which coalesce almost immediately to form the threadlike structures (or interconnected wormlike micelles) shown in panel B (at $t = 4$ ns) and C (at $t = 20$ ns). This irregular structure transforms itself into a single aggregate reminiscent of a bicelle (D, $t = 80$ ns)), i.e., a bilayer structure with curved edges. For a lamellar phase preferring lipid as DPPC the curved edges give rise to a large line tension. The line tension is subsequently minimized by gradually encapsulating water, leading to a cuplike vesicle containing a small pore (E, $t = 200$ ns). Eventually, the pore disrupts resulting in the vesicle shown

(13) Rawicz, W.; Olbrich, K. C.; McIntosh, T.; Needham, D.; Evans, E. *Biophys. J.* **2000**, *79*, 328.
(14) Zhelev, D.; Needham, D. *Biochim. Biophys. Acta* **1993**, *1147*, 89.
(15) Leontiadou, H.; Mark, A. E.; Marrink, S. J. *Biophys. J.* **2003**, in press.
(16) Sheats, J. R.; McConnell, H. M. *Proc. Natl. Acad. Sci. U.S.A.* **1978**, *75*, 4661.
(17) Kuo, A. L.; Wade, C. G. *Biochemistry* **1979**, *18*, 2300.
(18) Lindahl, E.; Hess, B.; van der Spoel, D. *J. Mol. Mod.* **2001**, *7*, 306.

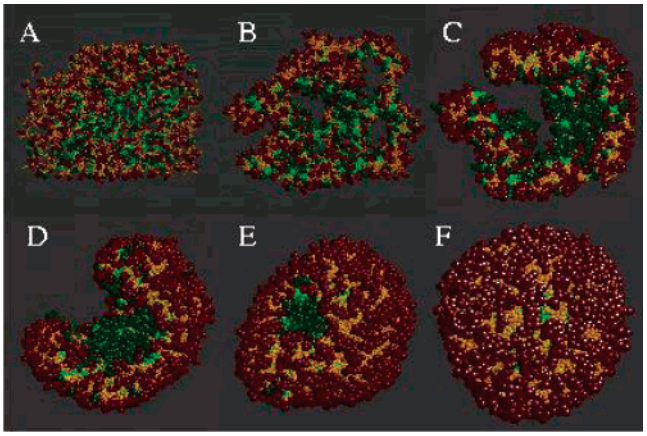

Figure 3. Aggregation process of DPPC lipids from a random solution into a vesicle. Red/orange colors are used to depict the head/tail groups of the lipids that end up in the outer monolayer, and dark green/light green colors for those ending up in the inner monolayer. Water is not shown for clarity. Snapshots are shown at $t = 0$ ns (A), 4 (B), 20 (C), 80 (D), 200 (E), and 240 ns (F). See text for details.

in panel F ($t = 240$ ns). The vesicle remained stable during the remainder of the 1 μs simulation.

Figure 4 highlights the closing of the final water pore, sealing the vesicle. Similar to what is found in the intermediate stages of bilayer formation,[19] the water pore has an hourglass shape. The interior of the pore is lined with the lipid headgroups. In contrast to the case of the bilayer formation process, however, a long living metastable state is not observed. The pore continues to decrease in size up till the point it disappears.

Figure 5 illustrates the forces that drive the vesicle formation process. In this figure we show the time dependence of the so-called Minkowski functionals, which are morphological measures describing the topology of the system (generally applied to characterize patterns in statistical physics, e.g., ref 20). For a three-dimensional system, there are four independent Minkowski functionals: the volume V, the surface area S, the average mean curvature H of the surface, and the Euler characteristic χ. Apart from the volume, which remains essentially constant throughout the simulation due to the very small compressibility of the phases, the other three measures are very sensitive to changes in topology. The surface of the lipid aggregate was obtained from dividing the system into small cubic volume elements of size 0.5 nm^3, corresponding to the size of the CG atoms. Each volume element was assigned to be of either lipid type or water type, depending on the relative density of the constituents inside. A 100-ps time average was used to smooth the spatial distribution. Volume elements of type lipid bordering those of type solvent were subsequently characterized as surface elements. The surface area S thus represents the interfacial area between the lipid and aqueous phase. The average mean curvature H and Gaussian curvature K of the interfacial area were obtained from the same set of volume elements using the procedure of Hyde et al.[21] The Euler characteristic (or Euler number) is related to the average Gaussian curvature via $\chi = 1/2\pi \int\int K\mathrm{d}S$. It can take integer values only, and reflects the connectivity of the system.

From Figure 5, it can be seen that both the surface area and the mean curvature of the aggregate surface are minimized during the formation of the vesicle. The minimization of the surface area is expected based on the surface tension that exists between lipids and water. Any increase in surface area would increase the free energy of the system. Because DPPC is a lipid that, under the simulation conditions, favors a lamellar phase with zero spontaneous curvature, the minimization of the total mean curvature is also expected to be a strong driving force. Zero curvature cannot be obtained for this system; however, unless the vesicle could fuse with its own periodic image and form a periodic lamellar bilayer. The excess solvent around the vesicle prevents this from happening. The line tension arising from the solvent exposed and strongly curved edges of the bicelle is apparently strong enough to overcome the bending energy required to form the vesicle. The value of the Euler characteristic clearly indicates the different topological stages of the formation process. Initially, the value is large and positive,

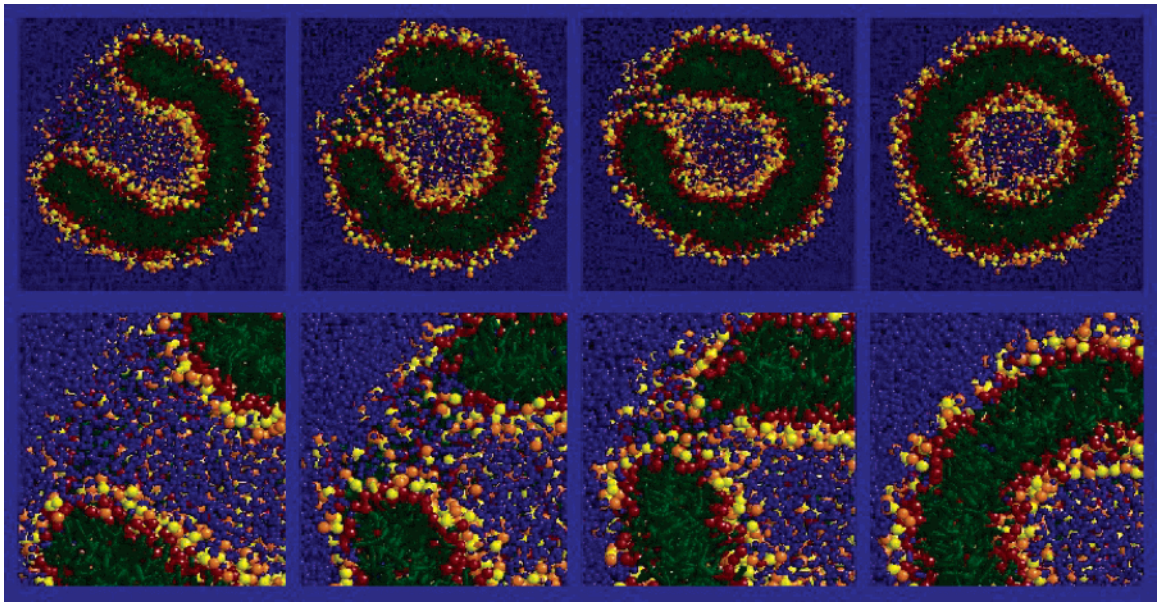

Figure 4. Close-up of the sealing of the vesicle. Snapshots are shown (from left to right) at $t = 180$, 200, 210, and 215 ns. The choline groups are colored orange, the phosphate groups yellow, the glycerol backbone dark red, and the tail groups green. Water is colored in blue. The bottom panel represents enlargements of the upper panel.

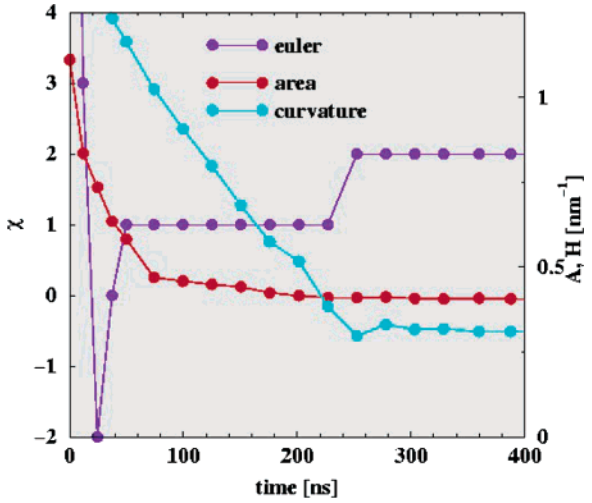

Figure 5. Time dependence of Minkowski functionals during the aggregation process. In purple is shown the Euler characteristic χ, in red the surface area A (expressed as surface-to-volume ratio), and in cyan the average mean curvature H of the interface.

indicating many unconnected sub-aggregates. The Euler characteristic rapidly decreases, and even becomes negative for a short period of time. At this stage, all of the sub-aggregates have merged into one large aggregate, which however contains holes (see snapshot B of Figure 3). The presence of holes results in a negative Euler number. When the holes are sealed, a single solid aggregate (the bicelle) remains, with an Euler number equal of 1. When this aggregate encapsulates water, however, an internal volume is pinched off from the surrounding medium, and the topology changes once more. The final vesicle is topologically equivalent to a hollow sphere, which has an Euler characteristic of 2.

Three of the four other simulations starting from random DPPC solutions follow the same general aggregation pathway, i.e., random solution−interconnected worms−bicelle−cuplike vesicle−vesicle. Also, the dynamics of the process is not very sensitive to the starting structure. Complete vesicles always formed between 200 and 300 ns. In each case, the vesicles remain stable during the remaining simulation time. In the simulation RANDOM-IV, which has a much higher lipid concentration, the final state is a hemifused vesicle rather than a single vesicle (see the next section). In this case, the system initially formed two bicellar like intermediates. During the process in which they started to encapsulate water, the two aggregates fused with each other. The resulting hemifused vesicle (formed after 200 ns) also remained stable for a subsequent 400 ns simulation. The high lipid concentration of this system is likely to be the reason for the different end structure. In the BICEL simulations, which started from a bicellar starting structure rather than from a random solution, the same bicelle to vesicle transition is observed as in the RANDOM simulations. The stage between the appearance of the bicelle (defined here as the moment the Euler characteristic increases to $\chi = 1$) in the RANDOM case, or the start of the simulations in the BICEL case, and the formation of the sealed vesicle ($\chi = 2$) ranges between 120 and 200 ns for the pure DPPC systems

(19) Marrink, S. J.; Mark, A. E. *J. Phys. Chem. B* **2001**, *105*, 6122.
(20) Mecke, K. R. *Phys. Rev.* **1996**, *E 53*, 4794.
(21) Hyde, S. T.; Barnes, I. S.; Ninham, B. W. *Langmuir* **1990**, *6*, 1055.

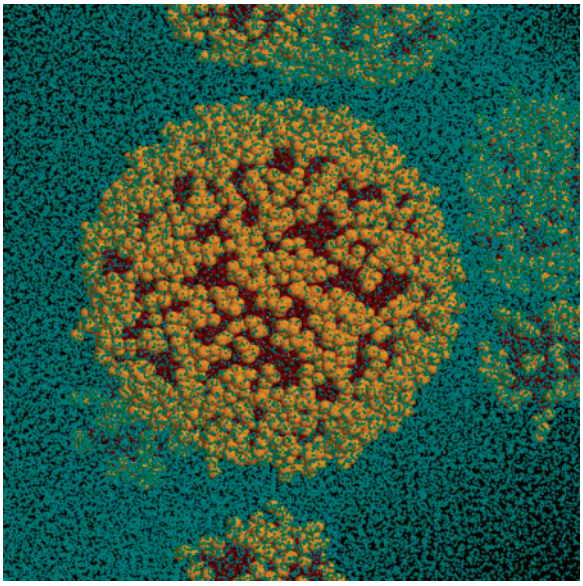

Figure 6. Close up of the final distribution of lipids of system RANDOM-I. The lipid headgroups are colored yellow, the rest of the lipid red. Water is colored in blue. The large aggregate is a small vesicle. The smaller aggregates are either micelles or very small dry vesicles.

Both mixed systems BICEL-PE-I and BICEL-lysoPC (started from the same bicellar structure) underwent a bicelle to vesicle transition similar to the pure DPPC systems. However, the dynamics of the bicelle to vesicle transition appeared significantly faster. In the mixed system, the transition time was 40 ns and 60 ns for aggregates containing PE and lysoPC respectively, three to four times faster than observed for the pure DPPC systems. Noticeably, the rim of bicelle, and later that of the pore, becomes enriched in lysoPC during the transition. The large headgroup of lysoPC with respect to its tail volume clearly favors the positive curvature of the bicellar edges and pore rim. For PE the opposite tendency is observed, although not as clearly as for lysoPC. The larger mixed PC/PE bicelle in system BICEL-PE-II, containing three times more lipids, required 250 ns to complete the transition to a sealed vesicle.

3.2 Structure of DPPC Vesicles. Figure 6 shows the final structure of one of the systems (RANDOM-I). The figure also shows that not all the lipids in the system managed to merge with the vesicle during the aggregation process. The remaining lipids are organized mainly in small micelles and sometimes in dry vesicles, i.e., vesicles of minimum size (~150 lipids, 7−8 nm diameter) only containing some hydration water but not containing any interior bulk water. The RANDOM-I simulation was extended up to 1 μs in order to see if any of the smaller aggregates would fuse with the vesicle. This did not happen. Table 3 summarizes the structural characteristics found for the vesicles formed during the various simulations. As mentioned in the previous section, in the simulation RANDOM-IV which has a higher lipid concentration, a hemifused vesicle was formed. In the simulation RANDOM-III the vesicle fused with a small micellar aggregate during the bicelle-to-vesicle transition. Complete merging of the micelle with the vesicle was not observed, however. At the end of the simulation part of the original micelle still sticks to the outer monolayer of the vesicle.

The vesicle formed in the simulation RANDOM-I contains 877 lipids, 251 (29%) of them residing in the inner monolayer.

Table 3. Structural Characteristics of Formed Vesicles

label	no. lipids	inner monolayer	interior water[a]	inner diameter ± 0.1 (nm)	outer diameter ± 0.1 (nm)
RANDOM-I	877 PC	251	914	6.3	13.4
RANDOM-II	893 PC	255	936	6.4	13.5
RANDOM-III[b]	1176 PC	321	1404	7.0	14.2
RANDOM-IV[c]	2500 PC				
BICEL-I	877 PC	245	913	6.3	13.5
BICEL-II	877 PC	248	917	6.3	13.4
BICEL-III	877 PC	252	909	6.4	13.5
BICEL-PE-I	877 (658 PC/219 PE)	251 (175/76)	750	6.0	13.4
BICEL-PE-II	2528 (1888 PC/640 PE)	947 (695/252)	8160	12.8	20.4
BICEL-lysoPC	877 (658 PC/219 lysoPC)	231 (179/52)	748	5.6	13.5

[a] Number of CG water particles. The corresponding number of real water molecules is four times larger. [b] A small micelle is semi merged to the outer monolayer of the vesicle. [c] a hemifused vesicle was formed in this simulation.

The structural composition of the vesicles formed in simulations BICELLE-I to -III, which started from the bicelle isolated from the RANDOM-I simulation is similar. The inner monolayers contained 245, 248 and 252 lipids respectively in these cases, resulting in an average of 249 (28.4%) with a standard deviation of only 3 (0.3%). The vesicles formed during the other two simulations which started from random solutions at the same overall lipid concentration, RANDOM-II and -III, are comparable in size. The fraction of inner monolayer lipids is 28.5% in the simulation RANDOM-II. In the simulation RANDOM-III the fraction is somewhat less (27.2%) but this is mainly due to the semi-merged micelle on its surface. The shape of the vesicle is close to a perfect sphere for each of the simulations (except for the hemifused vesicle obtained with the system RANDOM-IV). The amount of interior water molecules in the small vesicles is around 1000 CG particles, or four times as many real water molecules. Slightly more waters (1400) are inside the somewhat larger vesicle formed in the simulation RANDOM-III. The density of the interior water is 1 g cm^{-3}, equivalent to the density of the bulk water outside the vesicle.

The structure of the vesicle is further characterized by the radial distribution function (RDF) of the different components. The RDF is computed with respect to the center of mass of the vesicle, and is shown in Figure 7 for the simulation RANDOM-I (similar results are obtained for the other simulations of pure DPPC vesicles). For a graphical interpretation, compare to the structure of the final vesicle shown in the right panel of Figure 4. The distribution of the various groups is similar to that found in lamellar bilayers (see Figure 2), with two distinct headgroup layers separating the water phase from the carbon phase. As in lamellar bilayers, the water is found to penetrate into the glycerol backbone region, but not into the tail region. The characteristic dip in the density found both experimentally and computationally for the lamellar state is also present in the vesicle. The orientation of the phosphate−choline dipole vector is also similar to the orientation found in the lamellar state, i.e., mainly parallel to the membrane surface with the choline group pointing slightly outward. The diameter of the vesicles is around 14 nm measured from the peaks of the phosphate distributions. The inner diameter is close to 6 nm. Measured from the tails of the choline distribution, the diameter of the vesicle increases to 16 nm. Interestingly, the phosphate−phosphate thickness of the vesicular bilayer is 3.6 ± 0.1 nm, somewhat smaller than the value of 4.0 ± 0.1 nm obtained for the lamellar phase (see Figure 2). This points to a small curvature effect on bilayer thickness, probably related to the tension (see the Discussion section).

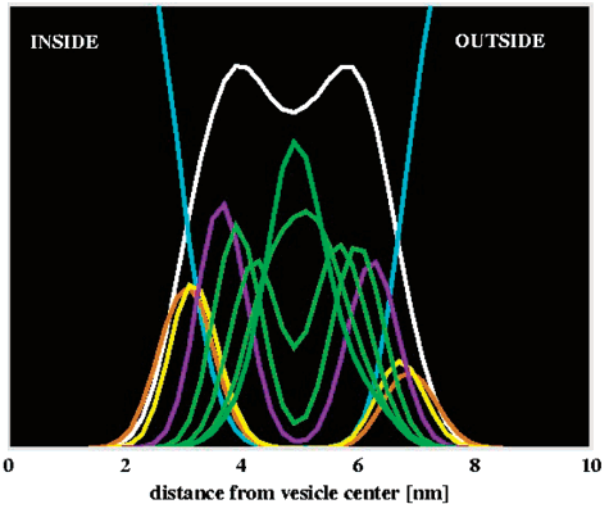

Figure 7. Radial distribution function of vesicle components. The RDF is computed with respect to the center of mass of the vesicle (at 0 nm on the ordinate). The water density is shown in blue, the density of NC3 groups orange, PO4 groups yellow, the glycerol backbone in purple, and each of the four tail groups in green. The total lipid density (scaled down) is shown in white. The bilayer midplane corresponds to a distance of 5 nm.

Although the distribution of the groups inside the vesicle appears similar to that inside a lamellar bilayer there is a significant difference between the inner and outer monolayers. The RDFs are not symmetric. Especially in the headgroup region the peaks in the distribution are much higher for the inner monolayer compared to the outer monolayer. The exterior water is able to penetrate the headgroup region of the vesicle to a larger extent. The tail region also shows some more subtle differences. Like the headgroups, the density for the first tail groups is higher in the inner monolayer. This trend is reversed for the third and fourth tail group, however. The origin of these effects can again be found in the curved nature of the bilayer. At the inner monolayer, the volume available per lipid is cone shaped, with a smaller volume available for the headgroups and a larger volume for the tails.

Figure 8 further emphasizes this point by showing RDFs separated for the inner and outer monolayers. The tails of the outer monolayer are shown to be distributed over a broader region compared to those of the inner monolayer. The terminal group of the outer monolayer is positioned, on average, almost in the middle of the bilayer. When compared to the inner monolayer lipids, the lipids in the outer monolayer appear more extended. At the same time however, a relatively high density is observed for the terminal groups near the phosphate group,

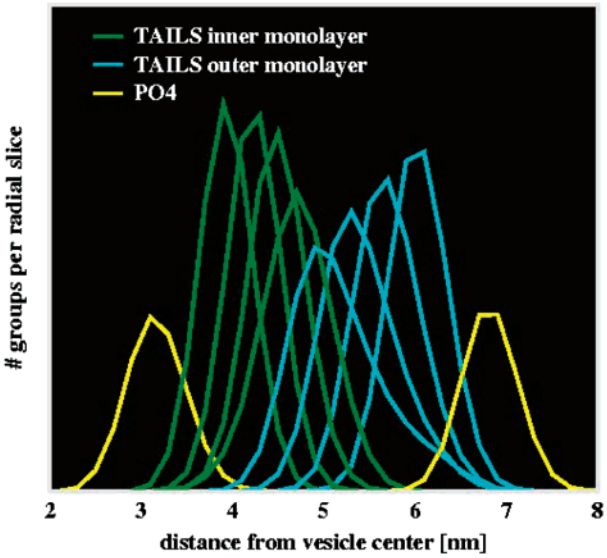

Figure 8. Radial distribution function per monolayer. The RDF is computed with respect to the center of mass of the vesicle (at 0 nm on the ordinate). RDFs of PO4 are shown in yellow, and of each of the tail groups of the inner monolayer in green, and of the outer monolayer in cyan. The bilayer midplane corresponds to a distance of 5 nm. The RDFs are multiplied by a factor r^2 to obtain the absolute number of groups found per radial slice. Furthermore, the RDFs of the inner monolayer are scaled with the ratio of the relative number of lipids in the outer monolayer versus the inner monolayer, to compare the relative densities.

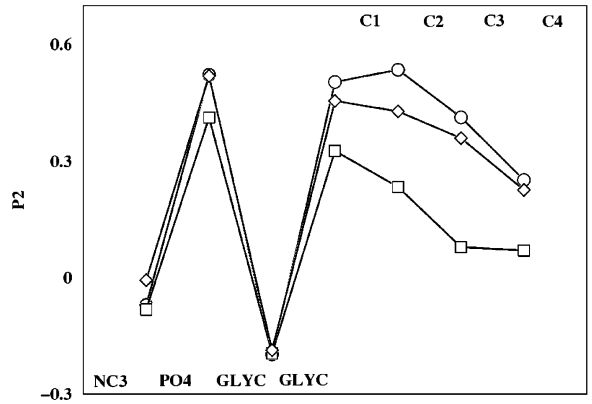

Figure 9. P_2 order parameter of consecutive bonds with respect to the surface normal. Results obtained for a pure DPPC vesicle. Inner monolayer data are marked with squares, outer monolayer data with diamonds. For comparison, circles indicate order parameters obtained from lamellar DPPC.

pointing to a higher degree of backfolding of the chains in the outer monolayer. To quantify the packing of the lipids further lipid order parameters are shown in Figure 9. The second-rank order parameter $P_2 = \langle 1/2\ (3\cos^2\theta - 1)\rangle$ was computed for consecutive bonds, with θ the angle between the direction of the bond and the vector connecting the center of the bond to the center of mass of the vesicle. Perfect alignment with the radial vesicle axis (or surface normal) is indicated by $P_2 = 1$, perfect anti-alignment with $P_2 = -0.5$, and a random orientation with $P_2 = 0$. For comparison order parameters were also obtained from a CG simulation of lamellar DPPC. The overall shape of the profiles is similar. Both the phospate-choline bond and the glycerol linkage have a predominantly parallel orientation with respect to the surface normal, whereas the other bonds prefer aligning along with the surface normal. Toward the end of the tails, the order decreases. A clear difference is observed for the order of the tail groups of the inner monolayer versus the outer monolayer, the former being much lower. The lipid tails of the inner monolayer are therefore more disordered. Compared to a lamellar system, also the outer monolayer tail groups appear more disordered. In contrast to the tail groups, the conformation of the lipid headgroups appears much more concerted. In the Discussion section, we introduce a simple packing model that can account for the above observations.

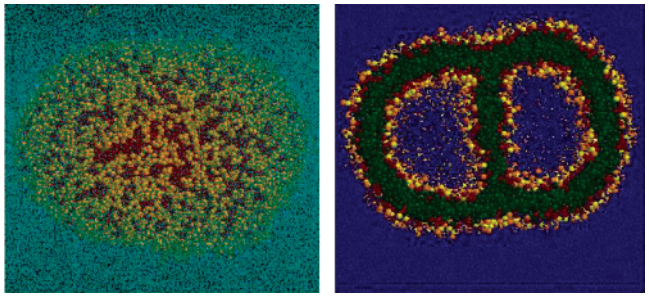

Figure 10. Snapshot of the hemifused vesicle formed spontaneously at high concentration (system RANDOM-IV). The right panel shows a cut through the middle. Color scheme as in figure 4. The hemifused vesicle is formed at very high lipid concentration, and remains stable during the simulation time (600 ns).

The structure of the other pure vesicles (RANDOM-II,III and BICEL-I−III) is found to be very similar. As described in the aggregation section, however, the lipids in simulation RANDOM-IV form a hemifused vesicle. The structure of the hemifused vesicle is shown in Figure 10. The hemifused vesicle contains all of the lipids present in the system, i.e., 2500. The cut through the middle of this vesicle shows that the system consists of two smaller vesicles that are trapped in the so-called hemifused state. In this state, the vesicles share one mutual bilayer that separates the contents of the two vesicles. According to the stalk-pore mechanism of membrane fusion (e.g., refs 22,23), this state corresponds to the last intermediate state during fusion. Rupture of the connecting membrane would be required to accomplish complete fusion of the two vesicles. This is not observed on the time scale of the simulations. It is interesting to point out the ability of the lipids to fill up the voids that theoretically would appear at the connection of three bilayers. Apparently, the lipids are flexible enough to tilt their tails slightly so as to avoid the energetically unfavorable creation of voids. This was also found in recent simulations of a cubic-hexagonal phase transition of glycerol monoolein lipid molecules,[24] and is in accordance with recent theoretical predictions.[22,25]

4. Structure of Mixed Vesicles

The structure of the small mixed vesicles containing 25% DPPE (BICEL-PE-I) or 25% lysoPC (BICEL-lysoPC) is shown in Figure 11. The structure is further characterized by the RDFs which are shown in Figure 12. The mixed PC/PE vesicle contains 251 lipids in the inner monolayer (28.6% of the 877 lipids altogether), which is similar to the pure DPPC vesicle. The relative amount of PE is higher in the inner monolayer, however, 30% versus 23% (overall concentration of PE is 25%). This can be understood in terms of the negative curvature of the inner monolayer versus a positive curvature for the outer

(22) Kozlovsky, Y.; Chernomordik, L. V.; Kozlov, M. M. *Biophys. J.* **2002**, *83*, 2634.
(23) Jahn, R.; Grubmuller, H. *Curr. Op. Cell Biol.* **2002**, *14*, 488.
(24) Marrink, S. J.; Tieleman, D. P. *Biophys. J.* **2002**, *83*, 2386.
(25) Kuzmin, P. I.; Zimmerberg, J.; Chizmadzhev, Y. A.; Cohen, F. S. *Proc. Natl. Acad. Sci. USA* **2001**, *98*, 7235.

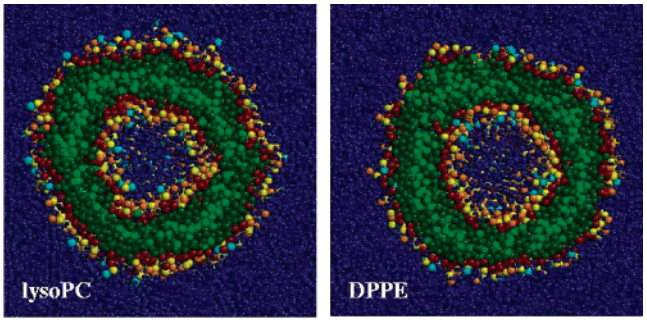

Figure 11. Snapshot of the interior of the mixed vesicles. Left: system BICEL-lysoPC containing 25% lysoPC−75% DPPC, and right: system BICEL-PE-I containing 25% DPPE−75% DPPC. Color scheme as in Figure 4. The NC3/NH3 groups of the minority component are shown in light blue. Terminal tail groups are colored a lighter shade of green. The outer monolayer is enriched in lysoPC, whereas the inner monolayer is enriched in DPPE. Note also the lysoPC headgroup protruding out of the surface, whereas the PE headgroup seems more condensed.

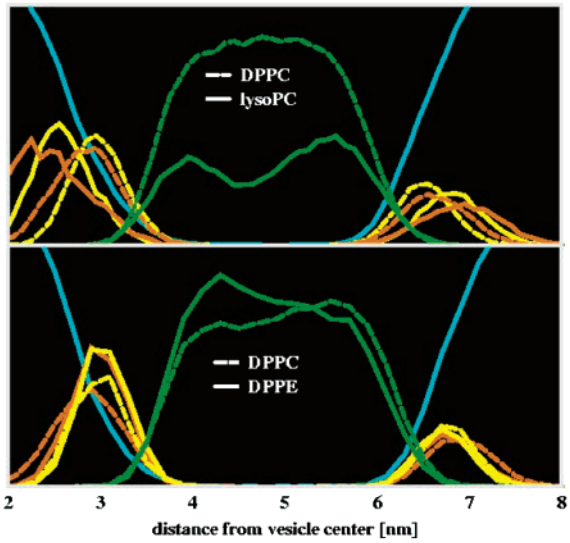

Figure 12. Radial distribution functions for the mixed vesicles shown graphically in Figure 11. The upper graph applies to the system BICEL-lysoPC containing 25% lysoPC−75% DPPC, the lower one to the system BICEL-PE-I containing 25% DPPE−75% DPPC. Solid lines are used for DPPE and lysoPC, dashed lines for DPPC. The RDF of the NC3/NH3 groups is shown in orange, PO4 in yellow, the TAIL groups in green, and water in cyan. The RDFs of the components are normalized by the bulk concentrations of the groups considered.

monolayer. Due to its smaller headgroup and inter headgroup hydrogen bonding capability, DPPE favors inverted phases (i.e., phase with negative curvature) compared to DPPC. Although in the CG model the NH3 is modeled with the same size as the NC3 group, the interactions with other headgroup atoms are much more attractive, making it effectively smaller. The mixed PC/lysoPC vesicle contains only 231 lipids in the inner monolayer (26.3%), a significantly smaller amount compared to the other vesicles composed of the same total number of lipids. LysoPC is also distributed asymmetrically across the two monolayers, with the higher percentage found in the outer monolayer (26% versus 23%).

The RDFs plotted in Figure 12 show a small difference between the packing of DPPC and either DPPE or lysoPC inside the bilayer. Apart from the asymmetric distribution of the lipids outlined above, it can be seen that the headgroup of lysoPC protrudes further out of the surface than does the DPPC headgroup. The NC3 group of the DPPC headgroup, in turn,

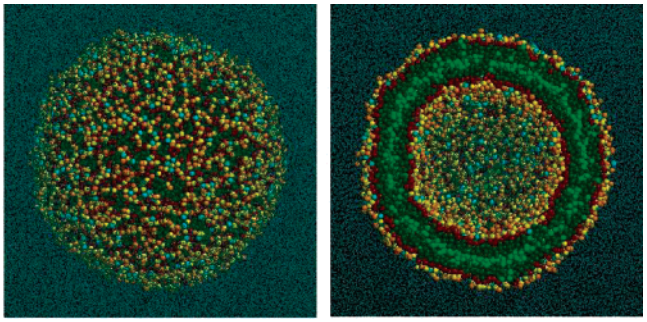

Figure 13. Snapshot of the large mixed DPPC/DPPE vesicle (system BICEL-PE-II). The right panel shows a cut through the middle. Color scheme as in Figure 11.

protrudes out of the surface to a greater extent than the NH3 group of PE. The dipole of the PE headgroup lies in the plane of the membrane, as is also observed in atomistic MD simulations of mixed PC/PE bilayers (de Vries, personal communication). The outer radius of the mixed PC/PE vesicle is not significantly different from those found for the pure vesicles. The inner radius is somewhat smaller (3.0 versus 3.2 nm), and therefore the thickness somewhat larger (3.8 versus 3.6 nm). This is a result of the condensing effect of PE on the lipid area, which is also seen in atomistic simulations. The inner radius is even smaller for the PC/lysoPC system (2.8 nm). With an outer radius comparable to that of the other vesicles the bilayer thickness is even larger (3.9 nm), an effect that is mainly caused by the protusions of lysoPC. Due to the smaller internal volume, the water content of both type of mixed vesicles is less than that of the pure vesicles.

The structural details of the larger mixed PC/PE vesicle (BICEL-PE-II) are qualitatively similar to those obtained for the smaller vesicles. Containing approximately three times more lipids, the diameter of the vesicle formed increases to 20.4 nm. The inner radius is 12.8 nm, leaving space for 8160 CG water molecules inside. As a natural consequence of the larger radius, the relative amount of lipids in the inner monolayer (37%) is larger than for the small vesicles (∼28%). The structural differences between the inner and outer monolayer are therefore not as pronounced as observed for the small vesicles. The inner monolayer, for instance, is still enriched in PE but to a lesser extent (27% vs 30% in the smaller vesicle). Figure 13 shows the overall appearance and the inside structure of the large vesicle.

5. Vesicle Dynamics

The shape fluctuations and bilayer undulations of the small vesicles are very limited, and are therefore not analyzed in further detail. During the μs simulations of the isolated vesicles, the lipids are, however, able to diffuse across the surface of the vesicle to a large extent. We compute a value of $2.5 \pm 0.1 \times 10^{-7}$ cm^2 s^{-1} for the lateral diffusion coefficient of the lipids in the inner monolayer, and $4.8 \pm 0.1 \times 10^{-7}$ cm^2 s^{-1} for those residing in the outer monolayer of the pure DPPC vesicle. These values were computed from the slope at short times (between 5 and 50 ns) of the mean squared displacement, to avoid the effect of curvature. The outer lipids are seen to diffuse almost twice as fast as the inner ones, an observation that can be linked to the fact that the headgroups of the lipids in the inner monolayer are much more densely packed (see Figure 7). The

diffusion rate for lamellar DPPC modeled with the CG approach at the same temperature is $3.2 \pm 0.1 \times 10^{-7}$ cm^2 s^{-1}, a value intermediate between the two vesicular monolayers. The process of flip-flopping of lipids from one leaflet to the other was not observed on the microsecond time scale of the simulations. After the sealing process of the vesicles has finished, the lipids remain in the same monolayer.

From the long BICEL-I simulation we have also gathered statistics concerning the exchange of interior and exterior water. The outward flux of water through the vesicle equals $J = 80 \pm 25$ CG water particles per μs. The leaking water molecules are replaced by an equivalent inward flux, i.e., no significant swelling or shrinking of the vesicle is observed. Using the relation $P = J/\Delta CA$, where ΔC denotes the water concentration and A the surface area of the lipid vesicle, the permeability coefficient P of the vesicle is estimated to be of the order of $P = 10^{-3}$ cm/s. This number is of the same order of magnitude as the experimentally measured permeability coefficients for pure DPPC vesicles.[26,27]

6. Discussion

We show that the formation and structure of (small) vesicles can be studied at near-atomic detail by coarse grained molecular dynamics simulations. In contrast to previous studies which either ignore explicit solvent contributions or use dissipative particles which can overlap, our model is more realistic. Therefore, both the structural and dynamic information obtained in the current simulations can be interpreted on a quantitative rather than only on a qualitative level.

We observe the formation of small unilamellar vesicles on a nanosecond time scale, which is very fast compared to experimental measurements of vesicle formation. Experimentally, vesicles are usually obtained by sonication of multilamellar aggregates—only certain lipids or lipid mixtures spontaneously form vesicles. For the setup chosen in the simulation, however, a (multi) lamellar state is unreachable, and the vesicular phase is preferred. Due to the high local lipid concentration the thermodynamic forces driving aggregation are very high, leading to self-assembly on a nanosecond time scale. Similar time scales were observed in previous studies of micelle[28] and bilayer[4] formation using atomistic models. The initial clustering of lipids even occurs on a subnanosecond time scale at the concentrations studied in this paper. Lipid clusters of various sizes form. Due to the limited total amount of lipids present in the simulation, only the largest carries enough mass to actually form a vesicle. The smaller clusters rearrange into micelles or, sometimes, dry vesicles (with no interior water apart from waters trapped in the lipid hydration shells). Fusion events of these smallest cluster with the largest vesicle-forming aggregate are usually not observed on the time scale of the simulations, indicating that such processes require longer than microseconds. The largest aggregate formed initially resembles a collection of interconnected wormlike micelles. These quickly rearrange and reduce the excess of surface area and curvature to form a bicelle. The bicelle can further reduce its curvature and surface area by encapsulating water, forming a cup-like vesicle. Upon the closing of the final water pore, a sealed vesicle is formed. This sequence of events (interconnected worms, bicelle, cup-like vesicle, vesicle) appears universal, as it is also observed in the vesicle formation studies using stochastic models.[1−3] Bicelles and cup-like vesicles can also be trapped experimentally in the process of vesicle formation.[29] The bicelle-to-vesicle transition for the small vesicles that appear in the simulation occurs within tens of nanoseconds. It is therefore fast compared to the rate of lipid diffusion (lipids require tens of nanoseconds to diffuse past their nearest neighbors). However, the transition rate is strongly size dependent. Increasing the amount of lipids 3-fold, the rate is observed to drop by almost an order of magnitude. Interestingly, the transition rate is observed to increase when either PE or lysoPC are present. Possibly, the presence of a second lipidic component reduces the bending rigidity of the bilayers through an asymmetric distribution of the lipids between the two leaflets, facilitating its curvature. Compared to lysoPC, DPPE accelerates the sealing of the vesicle even further. Whereas positively curved lipids such as lysoPC are known to promote pore formation in bilayers, the opposite effect is expected for inverted type lipids such as PE.[6] PE thus effectively increases the line tension, which is the driving force of vesicle sealing.

Limited by the amount of lipids simulated, the vesicles studied in the present simulations are somewhat smaller than the smallest sizes that can be readily obtained experimentally.[5] For DPPC, the smallest vesicles observed experimentally have a diameter of ~20 nm, whereas most of the CG vesicles have a diameter of roughly 15 nm (except for one larger vesicle with a diameter over 20 nm). The fact that even the smallest CG vesicles spontaneously seal could be an effect of the over estimation of the line tension in the CG model. Compared to experimental measurements it is too high roughly by a factor of 5 (see the Methods section). The high curvature present in the coarse grained vesicles allowed us to study the subtle differences in packing between a vesicular and a lamellar phase. Not only because of the curvature effect being more pronounced in small vesicles than in large ones, but also because of the absence of large shape fluctuations and surface undulations. Larger vesicles at equilibrium are effectively in a tensionless state, whereas smaller vesicles are under tension due to the suppressed fluctuations. Due to this tension the vesicular bilayer of a small vesicle experiences a certain amount of stress. The thinning of the bilayer that we observe for the vesicular bilayer compared to the lamellar one can be understood from these principles. On the basis of the radial distribution functions of the various lipid components across the bilayer, and on the calculated order parameters, it is possbile to present a schematic model to illustrate the differences in packing between the inner and outer monolayer of a vesicle (Figure 14). This cartoon shows the relative volume elements occupied by the lipids in both inner and outer monolayer. For the inner monolayer, the volume element is of an inverted type, i.e., with a smaller amount of volume available for the headgroup compared to the tails. For the outer monolayer, this is the other way around. To compensate for the lack of tail volume for the lipids in the outer monolayer, we essentially observe three different mechanisms, illustrated in Figure 14. First, the volume element of the outer monolayer is stretched beyond the bilayer midplane toward the

(26) Carruthers, A.; Melchior, D. L. *Biochemistry* **1983**, *22*, 5797.
(27) Andrasko, J.; Forsen, S. *Biochem. Biophys. Res. Comm.* **1974**, *60*, 813.
(28) Marrink, S. J.; Tieleman, D. P.; Mark, A. E. *J. Phys. Chem. B* **2000**, *104*, 12 165.
(29) Lasic, D. D.; Joannic, R.; Keller, B. C.; Frederik, P. M.; Auvray, L. *Adv. Coll. Int. Sci.* **2001**, *89−90*, 337.

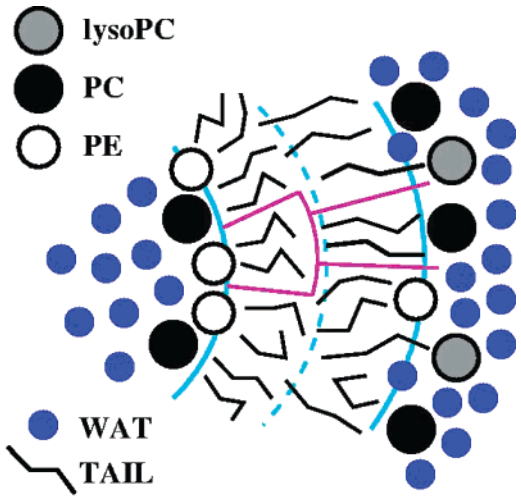

Figure 14. Representation of the lipid organization in small vesicles. The cyan lines denote the position of the water/lipid interface (solid) and the geometrical bilayer center (dashed). The average volume element occupied by the lipids in the inner and the outer monolayer is shown in purple. Three key features that solve the geometrical constraints are illustrated: (i) the outer monolayer is enriched in lysoPC and depleted of PE, (ii) the inner monolayer interface expels water, and (iii) the tails in the outer monolayer either extend beyond the midplane of the bilayer or fold back toward the interface.

inner monolayer. The additional volume available allows the terminal groups of the outer monolayer lipids to be distributed on both sides of the bilayer midplane, as can be deduced from Figure 8. The stretching of the lipid tails is clearly reflected in the high order parameters compared to those of the inner monolayer (see Figure 9). Second, a higher degree of backfolding is observed in the outer monolayer. This mechanism allows some of the tail groups to pack at or near the headgroup region, where a relatively large volume is available. In Figure 13, this effect clearly shows up as an increased amount of terminal tail groups (colored in light green) near the outer monolayer surface. The overall order in the outer monolayer is therefore smaller than in a lamellar phase. Third, in mixed systems, the outer monolayer is enriched in lipids with larger headgroups (PC instead of PE) or smaller tails (lysoPC instead of DPPC). Similarly, the lack of headgroup volume in the inner monolayer is solved by several mechanisms. First, the amount of interfacial water is reduced, leaving more space for the headgroups (Figure 7). Second, less backfolding is observed (Figure 8) also allowing the headgroups to pack more closely. Both effects result in a headgroup density of the inner monolayer almost twice as high as for the outer monolayer. The total lipid density however is similar in both interfacial regions (Figure 7). Third, the inner monolayer is enriched in inverted type lipids (PE) and depleted of positive curvature inducing lipids (lysoPC). This is also seen experimentally in mixed vesicles containing PE.[30] Although curvature effects are probably exaggerated due to the very high curvature present in the small vesicles simulated, we observe the same qualitative differences for the larger vesicle as well. Obviously, the distinction between inner and outer monolayer will vanish for macroscopically large vesicles. More generally, the packing mechanisms outlined above can be expected to be important in any nonlamellar bilayer phase, such as the cubic or hexagonal phases, or at the intermediate stages of bilayer fusion for instance. The packing details of the outer monolayer lipids are especially relevant to so-called type I lipids (which favor positive curvature), whereas the inner monolayer lipids resemble type II lipids (favoring inverted phases with negative curvature). A recent atomistic simulation of type II lipids (monoolein) in an inverted cubic phase[31] indeed reveals packing details similar to those obtained for the inner monolayer of the vesicles simulated. The effect of different lipids on the vesicle fusion mechanism will be published separately.[32]

JA0352092

(30) Sun, C.; Hanasaka, A.; Kashiwagi, H.; Ueno, M. *Biochim. Biophys. Acta* **2000**, *1467*, 18.
(31) Marrink, S. J.; Tieleman, D. P. *J. Am. Chem. Soc.* **2001**, *123*, 12 383.
(32) Marrink, S. J.; Mark, A. E. *J. Am. Chem. Soc.* **2003**, *125*, 11 144.